Calcium Binding and Ionic Conduction in Single Conical Nanopores with Polyacid Chains: Model and Experiments

Mubarak Ali,[†,‡,*] Saima Nasir,[†,‡] Patricio Ramirez,[§] Javier Cervera,[⊥] Salvador Mafe,[⊥] and Wolfgang Ensinger[†,‡]

[†]Department of Material- and Geo-Sciences, Materials Analysis, Technische Universität Darmstadt, D-64287 Darmstadt, Germany, [‡]GSI Helmholtzzentrum für Schwerionenforschung, D-64291, Darmstadt, Germany, [§]Departament de Física Aplicada, Universitat Politécnica de València, E-46022 València, Spain, and [⊥]Departament de Física de la Terra i Termodinàmica, Universitat de València, E-46100 Burjassot, Spain

ABSTRACT Calcium binding to fixed charge groups confined over nanoscale regions is relevant to ion equilibrium and transport in the ionic channels of the cell membranes and artificial nanopores.

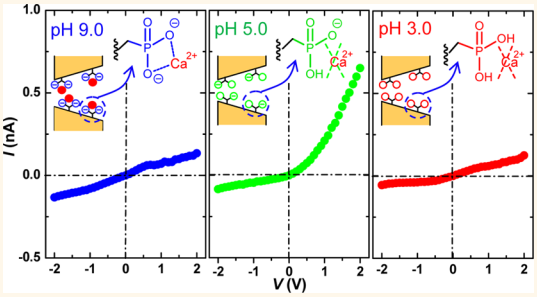

We present an experimental and theoretical description of the dissociation equilibrium and transport in a single conical nanopore functionalized with pH-sensitive carboxylic acid groups and phosphonic acid chains. Different phenomena are simultaneously present in this basic problem of physical and biophysical chemistry: (i) the divalent nature of the phosphonic acid groups fixed to the pore walls and the influence of the pH and calcium on the reversible dissociation equilibrium of these groups; (ii) the asymmetry of the fixed charge density; and (iii) the effects of the applied potential difference and calcium concentration on the observed ionic currents. The significant difference between the carboxylate and phosphonate groups with respect to the calcium binding is clearly observed in the corresponding current–voltage (*I*–*V*) curves and can be rationalized by using a simple molecular model based on the grand partition function formalism of statistical thermodynamics. The *I*–*V* curves of the asymmetric nanopore can be described by the Poisson and Nernst–Planck equations. The results should be of interest for the basic understanding of divalent ion binding and transport in biological ion channels, desalination membranes, and controlled drug release devices.

KEYWORDS: calcium binding · dissociation equilibria · conical nanopore · current–voltage curves

Calcium ions play a key role in cell biochemistry, being involved in plant growth and development, the modulation of cell death, and the regulation of neuronal excitability. Many biochemical processes involve the calcium binding and subsequent blocking/reduction of ionic currents that occurs in the ion channels.[1] Cyclic nucleotide-gated (CNG) ion channels activated by cyclic guanosine monophosphate/adenosine monophosphate (cAMP/cGMP) play a vital role in the visual and olfactory sensory systems of vertebrates.[2] These channels are cation selective and conduct different monovalent as well as divalent cations. However, under physiological conditions they preferably permeate Ca^{2+} ions due to the presence of specific binding site(s) in the selectivity filter of the pore.[3,4] The Ca^{2+} binding inside the pore effectively blocks the monovalent cation current,[5,6] leading to a reduction of channel conductance and playing a central role in the signal transduction of the visual system.[7] The binding of divalent and trivalent ions to internal sites is responsible for the gating of the current in many ion channels.[1−11]

The interaction between the charges fixed on the channel surface and the mobile ions in solution is usually crucial in the above phenomena. Remarkably, the ionic equilibrium and transport observed in artificial nanopores with pH-sensitive fixed charges confined over small volumes can mimic some of the processes characteristic of ion channels.[12−30] The nanoscale pores constitute then a convenient model to study the basic physical chemistry involved in the more complex biological phenomena. The control of the pore geometry and the surface functionalization allows some of the functionalities characteristic of wide ion channels.[12,14−16,20,31−35] Previous relevant studies have concentrated on different effects of calcium-induced voltage gating in narrow pores (current fluctuations and transient phenomena, negative incremental resistance and ratchet effects, precipitation-induced processes, and local charge inversion).[25,26,28,36]

We present here experimental and theoretical descriptions of the effects of calcium binding on ionic transport for the case of a

* Address correspondence to m.ali@gsi.de, m.ali@ca.tu-darmstadt.de.

Received for review August 13, 2012 and accepted September 16, 2012.

Published online September 17, 2012
10.1021/nn303669g

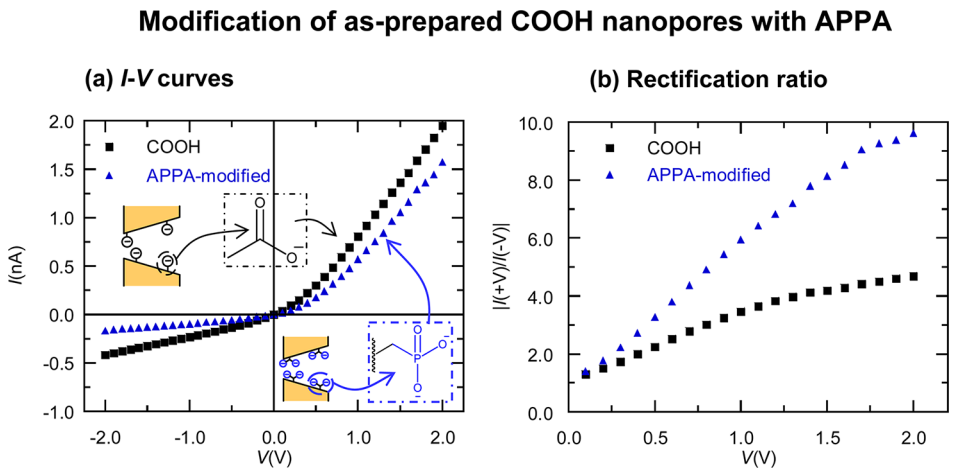

Figure 1. (a) Experimental *I*−*V* curves of a single conical nanopore measured in a 0.1 M KCl (pH = 9.0) aqueous solution prior to (■) and after (▲) modification with APPA molecules. (b) Rectification ratio obtained from the respective *I*−*V* curves.

single conical nanopore bearing ionizable carboxylic acid and phosphonic polyacid chains. The nanostructures are fabricated by means of the asymmetric track-etching procedure[29] and incorporate functional chemical (phosphonic acid) groups onto the pore surface and inner walls by the covalent coupling of surface carboxylic acid moieties with 3-aminopropylphosphonic acid (APPA) *via* carbodiimide coupling chemistry. The phosphonic acid groups display multiple pK_a values,[37] which generate different protonation/deprotonation states that can be modulated by the external solution pH. In fully ionized form, these groups act as binding sites for Ca^{2+} ions.

The high surface/volume ratio of the nanopore produces significant electrical double-layer effects on the calcium binding. Different phenomena are simultaneously present in this problem: (i) the nature (monovalent or divalent) of the charge groups fixed to the pore walls and the influence of the pH and calcium concentration on the reversible dissociation equilibrium; (ii) the asymmetry of the fixed charge density; and (iii) the effects of the calcium concentration on the current−voltage (*I*−*V*) curves. The significant difference between the carboxylate and phosphonate groups with respect to the binding phenomena is clearly observed in the *I*−*V* curves and can be rationalized by using a simple molecular model based on the grand partition function formalism of statistical thermodynamics. The results obtained involve basic physical and biophysical chemistry concepts and should be of interest for the understanding of divalent cation binding and transport in biological ion channels, desalination membranes, and controlled release units because of the calcium ion relevance and the fact that single pore tracks are the elementary constituents of membranes.[38−43]

RESULTS AND DISCUSSION

Experimental Results. Figure 1a shows the experimental *I*−*V* curve of a single, as-prepared conical nanopore with carboxylic acid (COOH) groups measured at concentration c_S = 0.1 M KCl in the external aqueous solutions. The *I*−*V* curve measured after pore modification with APPA molecules and the schemes of the pore chemical functionalities are also included. The value $I > 0$ corresponds to the cation flowing from the narrow (tip) toward the wide (base) opening of the conical nanopore. Figure 1b shows the rectification ratio obtained from the respective *I*−*V* curves of Figure 1a. The results of Figure 1a correspond to pH = 9.0, where the ionized carboxylate ($-COO^-$) groups are negatively charged and the anion (Cl^-) concentration is much lower than the cation (K^+) concentration in the pore solution. The high conductance state ($V > 0$) corresponds to the cations entering first the negatively charged cone tip, and the low conductance state ($V < 0$) corresponds to these carriers entering first the (almost neutral) cone basis. The increase in the fixed charge concentration of the APPA-modified pore with respect to the as-prepared pore causes a significant increase in the concentration of electrical carriers (the cations here), and then the ionic current rectification characteristic of the pore also increases (Figure 1a). The nanopore rectification characteristic is described by the ratio *r* between the electric current in the conductive and nonconductive pore states obtained at a given voltage. The ratios are $r \approx 5$ and $r \approx 10$ for the as-prepared and APPA-modified pore, respectively, at $V = 2$ V, in agreement with the high fixed charge concentration of the APPA-modified pore.

Figure 2 shows the experimental *I*−*V* curves and the charge state of the pore modified with APPA molecules in (a) the absence and (b) the presence of Ca^{2+} ions (1 mM $CaCl_2$) in the background electrolyte solution at the pH values indicated in the respective *I*−*V* curve. The pK_{a1} and pK_{a2} values of the two ionizable hydroxyl groups in the attached phosphonic acid ($-PO_3H_2$) moieties are ~4.5 and ~7.7, respectively.[37] The pH dictates the dissociation state of the weak acid moieties in the pore and thus is relevant for ionic equilibrium and transport properties.[13−15,38−40,43−45]

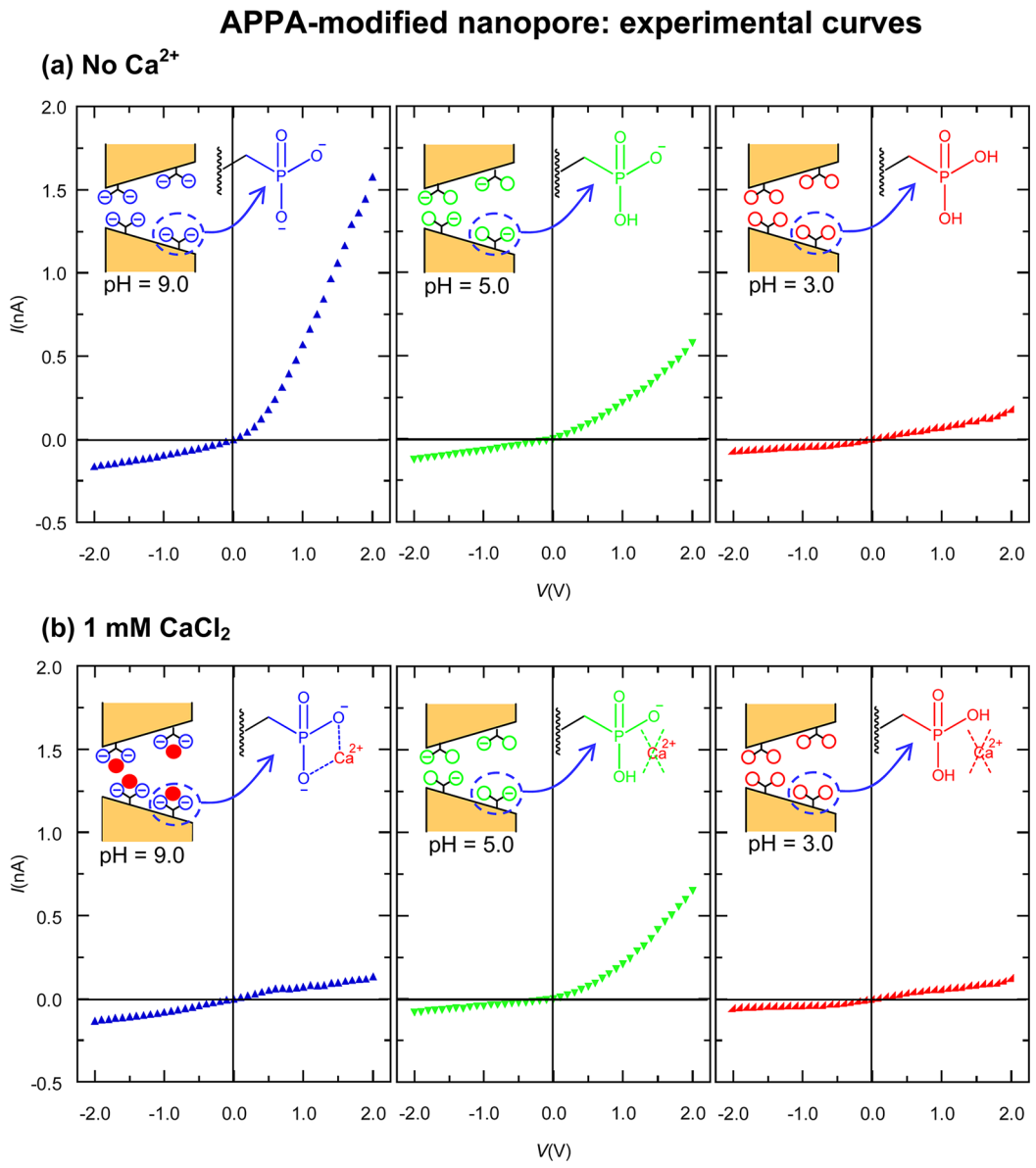

Figure 2. Experimental *I*−*V* curves of the nanopore modified with APPA molecules in (a) the absence and (b) the presence of Ca^{2+} (1 mM $CaCl_2$) in the electrolyte (0.1 M KCl) solution at the pH values indicated in the curves. The estimated pore dimensions are 12 μm (length), 260 nm (pore base diameter), and 6 nm (pore tip diameter).

The pH-dependent *I*−*V* curves of the modified nanopore in the absence of Ca^{2+} ions (Figure 2a) were discussed previously.[16] In alkaline conditions (pH = 9 > pK_{a2}), the fully ionized phosphonate ($-PO_3^{2-}$) groups produce high positive currents and rectification values. At intermediate pH conditions (pH = 5, $pK_{a1} < 5 < pK_{a2}$), the phosphonic ($-PO_3H^-$) groups give a negative charge density lower than the corresponding value at pH = 9 and then a decrease in the current (from 1.58 to 0.57 nA) and the rectification *r* (from ~10 to 4.6) values at +2 V. For the acidic condition pH = 3 < pK_{a1}, complete protonation of the phospohonic ($-PO_3H_2$) groups produces a neutral pore with a quasi-linear *I*−*V* curve (no rectification).

Figure 2b shows the experimental *I*−*V* curve of the modified nanopore in the presence of Ca^{2+} ions (1 mM $CaCl_2$) in the electrolyte (0.1 M KCl) solution under different pH conditions. It is evident from the *I*−*V* curves measured at pH = 3 and 5 that the Ca^{2+} ions do not induce any change in the ion transport through the pore when the phosphonic acid moieties are in fully ($-PO_3H_2$) and partially ($-PO_3H^-$) protonated states. Under these conditions, no binding of Ca^{2+} ions with the $-PO_3H_2$ and $-PO_3H^-$ groups occurs. On the contrary, at pH = 9 > pK_{a2}, at which the phosphonate ($-PO_3^{2-}$) groups are in the completely ionized state, a relatively low concentration of Ca^{2+} ions (1 mM) in the external solutions dramatically changes the *I*−*V* curve (note that the monovalent potassium K^+ ions are in the 100 mM range). The binding of Ca^{2+} with the divalent $-PO_3^{2-}$ group results in the neutralization of the pore charge, and consequently, the pore switches

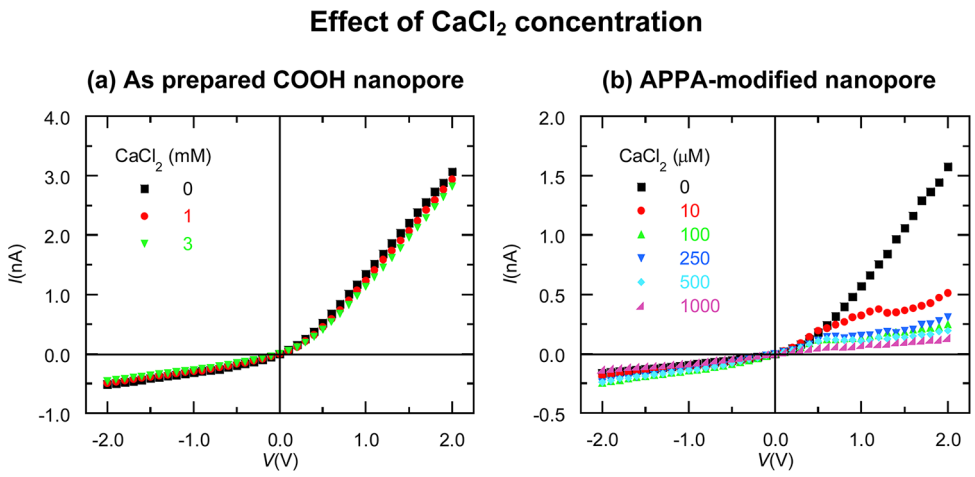

Figure 3. Experimental *I*−*V* curves of (a) the as-prepared COOH pore and (b) the APPA-modified pore at different $CaCl_2$ concentrations in a 0.1 M KCl (pH = 9) solution.

from the highly conductive state to the low conductive state. The Ca^{2+} binding decreases the ionic current carried by the K^+ ions, as observed in biological ion channels.[1,5,8,9] For example, the suppression of the monovalent cation current and the concomitant lowering of channel conductance have been noted in the CNG ion channels of rod photoreceptors upon the binding of Ca^{2+} ions with the glutamate residues in the pore.[6−10] However, the decrease of the current observed in our case should be ascribed to the decrease of the mobile ion concentration caused by the low charge density in the pore after neutralization rather than to the steric pore blocking (ionic occlusion) that occurs in the narrow ion-specific biological channels.

Remarkably, Ca^{2+} binding is absent at pH = 5, indicating that the binding constant is much higher for the doubly charged $-PO_3^{2-}$ groups than for the singly charged $-PO_3H^-$ ones (note the similarity of the two *I*−*V* curves (Figure 2) in the absence and presence of Ca^{2+} ions in the electrolyte solution at pH = 5). This fact clearly suggests that the binding constant should be much lower than 10^3 M^{-1} in this case, contrarily to the doubly charged $-PO_3^{2-}$ group case (pH = 9). The values in the range $10-10^2$ M^{-1} have indeed been previously reported[38−40,43−45] for monovalent (*e.g.*, $-COO^-$) groups. Finally, the pore is neutral at pH = 3, and the *I*−*V* curve is again quasi-linear.

Figure 3 shows the changes in the experimental *I*−*V* curves of the (a) as-prepared pore and (b) APPA-modified pore with $CaCl_2$ solutions of different concentrations prepared in the same electrolyte (c_S = 0.1 M KCl and pH = 9). As expected, calcium binding is absent in the case of the pore with monovalent $-COO^-$ groups (Figure 3a) at calcium concentrations in the 1 mM range. Contrarily, for the case of the modified pore bearing divalent $-PO_3^{2-}$ groups, binding occurs even at very low calcium concentration, leading to a drastic change in the current carried by K^+ ions from the tip toward the base of the conical pore. The presence of only 10 μM calcium led to a ~85% decrease in the ionic current at +2 V (Figure 3b). This fact suggests that the effective binding constant should be on the order of 10^5 M^{-1} in this case.

We may compare the effective Ca^{2+} binding constants found here with those of ion channels. For the singly charged $-PO_3H^-$ group, the binding constant should be lower than 10^3 M^{-1}. On the contrary, for the doubly charged $-PO_3^{2-}$ group, this constant should be on the order of 10^5 M^{-1}. Models describing the gating of single calcium-dependent potassium channels have considered low- and high-affinity sites with effective constants lower than 10^4 M^{-1} and higher than 10^7 M^{-1}, respectively, for Ca^{2+} binding.[8] Also, effective constants for Ca^{2+} binding in calcium channels are on the order of 10^2 and 10^6 M^{-1} for low- and high-affinity binding (see refs 9 and 10 and references therein). Some calcium channels[1] are inactivated when the concentration of Ca^{2+} rises above 10^{-7} to 10^{-6} M, suggesting binding constants on the order of 10^6 M^{-1}. It has also been reported previously that calcium binds to multiple carboxylate groups with very high effective binding constants.[25,26]

Note also the saturation (and, in some cases, small decrease) of *I* with *V* that occurs at high calcium concentrations, presumably because of some partial pore blocking.[26,27] The decrease in the ionic currents of Figure 3b is more pronounced for the more concentrated $CaCl_2$ solutions. Eismann *et al.* have also investigated the effect of different Ca^{2+} concentrations on the conductance of the CNG channel. By increasing the Ca^{2+} concentration, the observed current was progressively suppressed due to the binding of Ca^{2+} ions with the high affinity pore sites, blocking the monovalent cation current.[9]

Figure 4a shows the *I*−*V* curves of the APPA-modified nanopore obtained for asymmetric additions of Ca^{2+} in the left (cone tip) and right (cone base) external solutions. Clearly, the charge state of the narrow region around the cone tip, which is the zone where the electrical double layer effects are significant, dictates the calcium binding

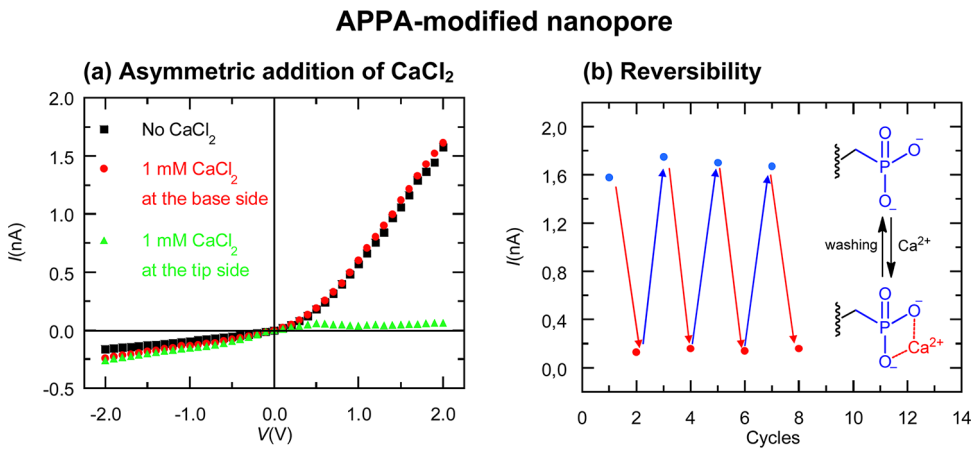

Figure 4. (a) $I-V$ curves of the APPA-modified pore with asymmetric addition of Ca^{2+} (1 mM $CaCl_2$) in the electrolyte (0.1 M KCl) solutions at pH = 9.0. (b) Ionic currents measured at 2 V upon reversible binding and unbinding of Ca^{2+} (1 mM $CaCl_2$) with the phosphonic acid groups of the APPA-modified pore during different cycles.

and the ionic transport.[23,32,46,47] It should be mentioned here that the rectification ratio of biological ion channels is also strongly dependent on the side of the channel where the blocking ion is added (examples concerning the ions Ca^{2+} and Mg^{2+} in potassium and calcium channels can be found in ref 1; a recent study concerning the ion La^{3+} in the bacterial porin outer membrane protein F, OmpF, channel can be found in ref 11).

Figure 4b shows the ionic currents obtained upon reversible binding and unbinding of Ca^{2+} with the doubly charged $-PO_3^{2-}$ groups in the modified nanopore. The currents observed for the different cycles after washing the pore show that the binding of Ca^{2+} with $-PO_3^{2-}$ groups is approximately a reversible process, in agreement with previous studies.[18]

Theoretical Results. Divalent ion binding to acid groups is significant in controlled drug delivery with ion exchange fibers,[38,39,43] ionic gels,[48] and the lipid bilayers of biological membranes.[1] We make use of a simple molecular model[45] based on the statistical thermodynamics formalism of Hill[49] and Ben-Naim[50] to estimate the number of effective (negative) charges in the phosphonic groups. The model has the advantages of simplicity and generality because it introduces only the minor structural information needed while providing some molecular background.[23,45]

Figure 5a shows the different states of the functional groups attached on the APPA-modified pore, and Figure 5b gives the grand partition function terms for these states. In this figure, λ_i is a magnitude proportional to the activity of ion i, and Z_i is the ionic partition function (including the binding energy).[45] The term corresponding to a phosphonic group with two negative charges is taken as unity (a reference value). From the grand partition function q, the average number θ_x ($0 \leq \theta_x \leq 2$) of effective charges in a phosphonic group is[45]

$$\theta_x = 2 - \theta_H - 2\theta_{Ca} = 2 - \lambda_H\left(\frac{\partial \ln q}{\partial \lambda_H}\right) - 2\lambda_{Ca}\left(\frac{\partial \ln q}{\partial \lambda_{Ca}}\right)$$
$$= \frac{2 + 2 \times 10^{pK_{a_1} - pH} e^{|\psi_D|}}{1 + 2 \times 10^{pK_{a_1} - pH} e^{|\psi_D|} + 10^{pK_{a_1} + pK_{a_2} - 2pH} e^{2|\psi_D|} + K_{Ca} c_{Ca} e^{2|\psi_D|}} \quad (1)$$

where we have taken into account that the pH value and the calcium concentration in the pore solution, which are denoted by overbars in Figure 5b, differ from those values in the external solution because of the Donnan factors $e^{|\Psi_D|}$ for hydrogen and $e^{2|\Psi_D|}$ for calcium, where[39,44]

$$|\psi_D| = \ln\left\{\frac{\theta_x X_0}{2c_S} + \left[\left(\frac{\theta_x X_0}{2c_S}\right)^2 + 1\right]^{1/2}\right\} \quad (2)$$

is the Donnan potential in RT/F units.[39] In eq 2, X_0 is the maximum value of the volume fixed charge concentration and $X = \theta_x X_0$ is the effective value of this concentration. Constants R, F, and T are the gas constant, the Faraday constant, and the absolute temperature, respectively. Note that the model involves only the volume fixed charge concentration X at the pore tip. It is the pore region where the interaction between the ions and the pore surface is more intense, and this interaction will eventually determine most of the nanopore characteristics.[23,32,47]

Figure 5c shows the effective charges in a phosphonic group calculated in the absence and presence of calcium for different values of the binding constant

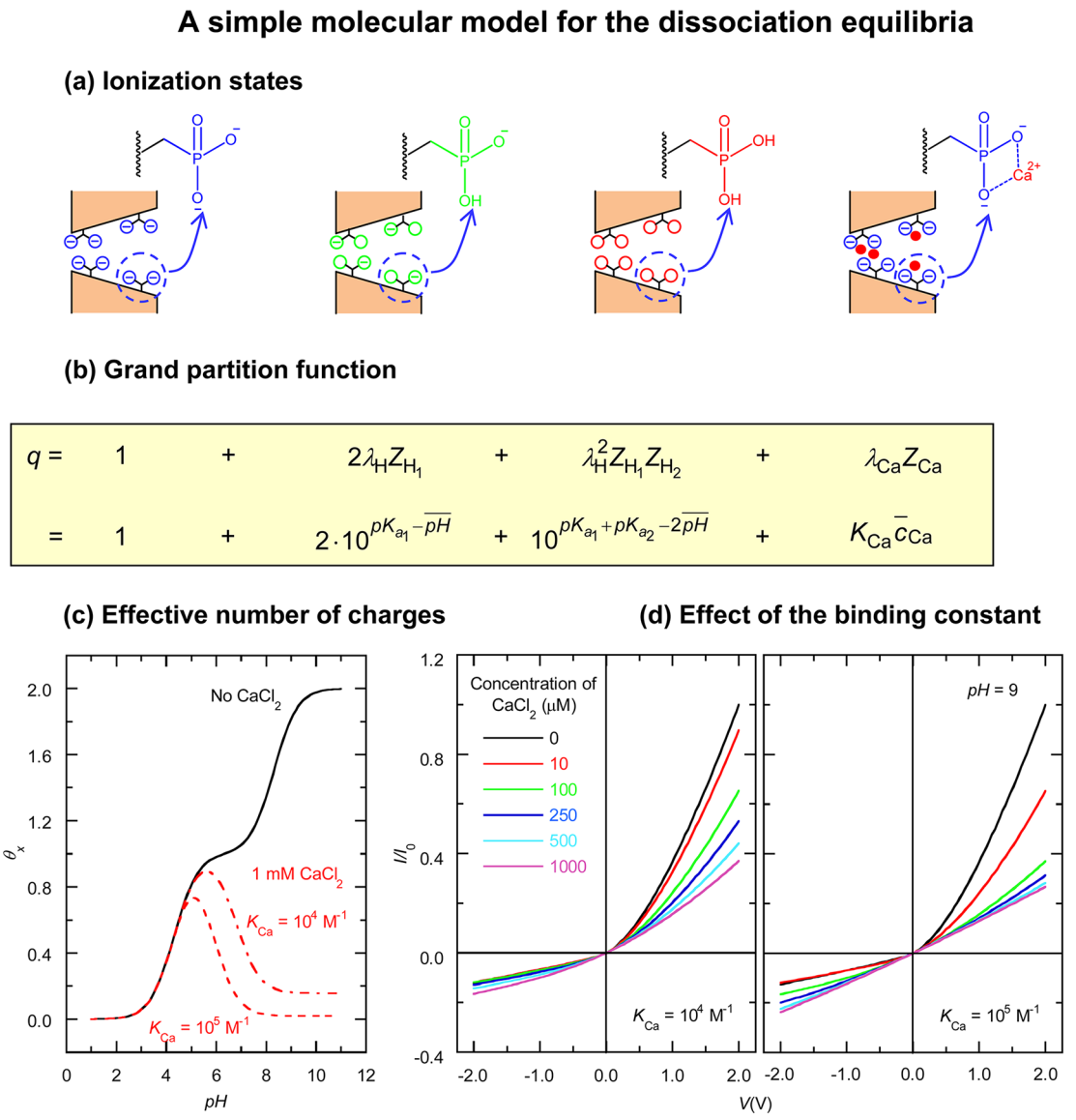

Figure 5. (a) Different ionization states of the functional groups attached on the APPA-modified pore. (b) Grand partition function for these states. The overbars denote the pH and calcium concentration values in the pore solution, which differ from those values in the external solution because of the Donnan equilibrium.[39,44] (c) Effective number of charges in a phosphonic group (θ_x) for the cases of the absence and presence of 1 mM $CaCl_2$ in the 0.1 M KCl electrolyte solution. The curves are calculated for two values of the binding constant K_{Ca}. (d) Influence of the binding constant in the theoretical $I-V$ curves for different $CaCl_2$ concentrations at pH = 9.0.

K_{Ca} with c_S = 0.1 M KCl. We have taken pK_{a1} = 7.7 and pK_{a2} = 4.5 according to previous results obtained with this nanopore functionalization.[14,37] The theoretical curves describe the dissociation equilibrium of the fixed charge groups as a function of the pH in the external solution and the assumed value for the calcium binding constant. In the absence of calcium, the double S-shaped curve describes the two successive deprotonations of the phosphonic group that occur approximately at the pH values given by the two pK_a values above. In the presence of calcium, the Ca^{2+} ions enter the pore from the external solution and compensate for the negative charges of the phosphonic groups (the effective number of negative charges per group is then lower than two). We have considered finally if the significant increase in the Ca^{2+} binding observed for the phosphonate groups might also be obtained by simply increasing the density X_0 in the case of the carboxylate groups. The fact is that doubling the density of the carboxylic groups while keeping the binding constant values significantly lower than those in Figure 5c has only a minor effect on the equilibrium (results not shown). It is the "electrostatic pocket" effect caused by the phosphonic groups on the Ca^{2+} ions (described here by the high values assigned to the effective binding constant) that determines the current decrease.

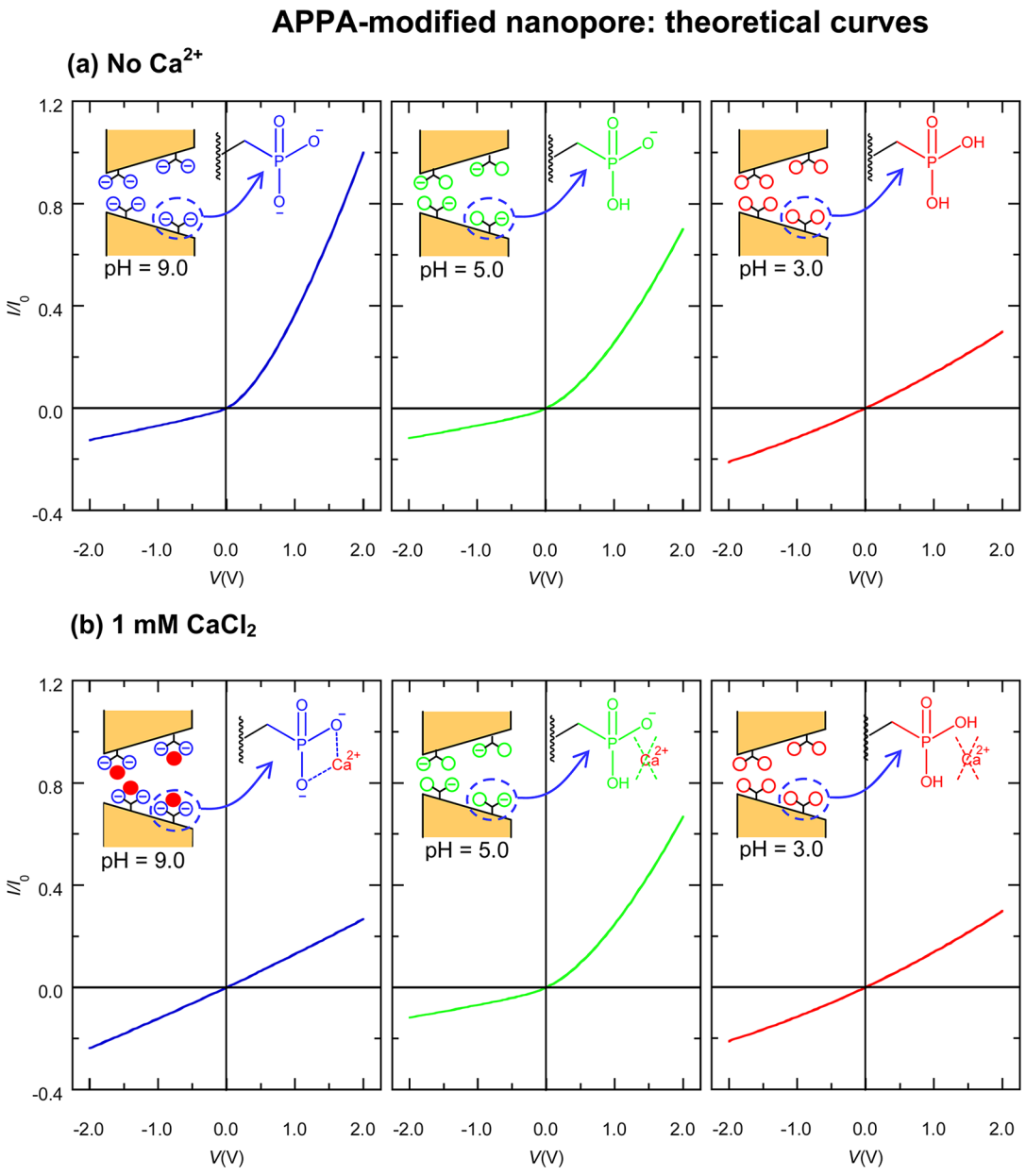

Figure 6. Calculated $I-V$ curves for a nanopore modified with APPA molecules in (a) the absence and (b) the presence of Ca^{2+} (1 mM $CaCl_2$) in the 0.1 M KCl electrolyte solution at different pH values. The current is scaled to a normalization current I_0 that depends on the nanopore and electrolyte solution characteristics.

The steady-state ionic transport is governed by the one-dimensional Nernst–Planck equations[14,38,51]

$$J_i = -D_i\left(\frac{dc_i}{dx} + z_i c_i \frac{F}{RT}\frac{d\phi}{dx}\right) \quad (3)$$

the Poisson equation

$$\frac{d^2\phi}{dx^2} = -F\left(\sum_i z_i c_i(x) - X\right)/\varepsilon \quad (4)$$

and the continuity equation

$$\frac{dJ_i}{dx} = 0 \quad (5)$$

where J_i, D_i, $c_i(x)$, and z_i are the flux density, the diffusion coefficient, the local concentration, and the charge number of ion i. The variable x denotes the axial pore coordinate, ε is the electrical permittivity, and $\phi(x)$ is the local electric potential. Note that we ignore the convective motion (electro-osmotic flow) of the fluid because it is the (narrow) cone tip that dominates the transport over the nanoscale volume.[41] In general, eqs 3–5 must be solved numerically, and details of the solution procedure can be found elsewhere.[32,47,51,52]

The results obtained with the above transport model are shown in Figures 5d and 6. We have introduced $D_i = 2 \times 10^{-9}$ m^2/s for all ionic diffusion coefficients and 12 μm (length), 260 nm (pore base diameter), and 6 nm (pore tip diameter) for the nanopore dimensions. The surface charge density $\sigma = 0.2\ e$ nm^{-2}, where e is the elementary charge,

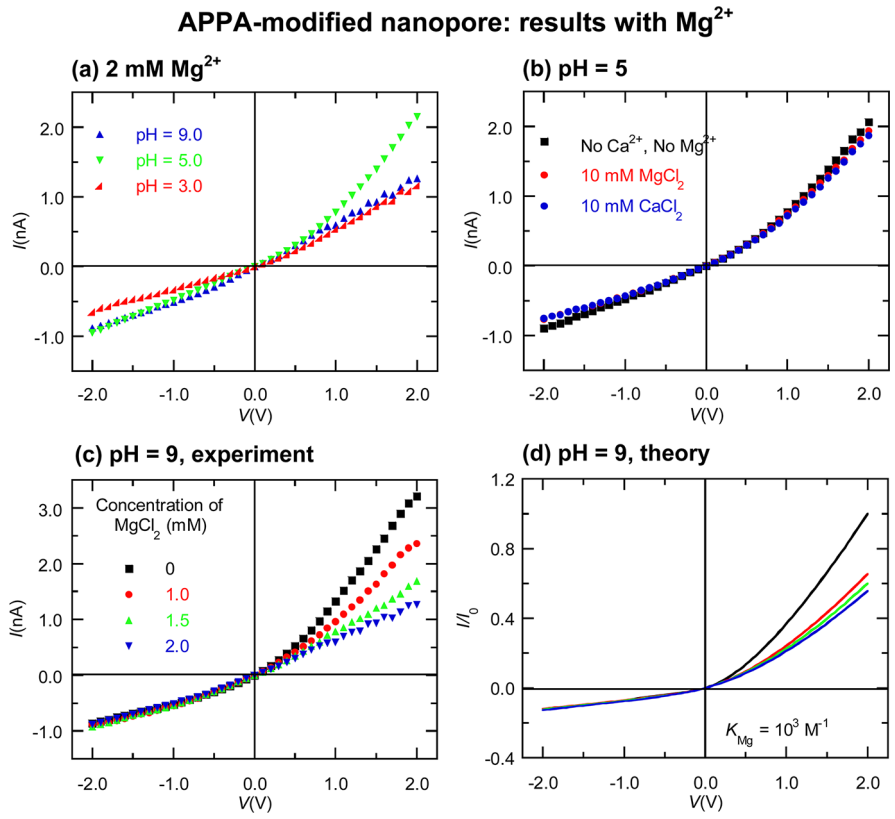

Figure 7. Experimental $I-V$ curves of (a) the APPA-modified pore at fixed $MgCl_2$ concentration (2 mM) at different pH, (b) the same pore in the absence and presence (concentration 10 mM) of ions Mg^{2+} and Ca^{2+} at pH = 5, and (c) the same pore at different $MgCl_2$ concentrations at pH = 9. In all cases, $c_S = 0.1$ M KCl. The estimated pore dimensions are 12 μm (length), 380 nm (pore base diameter), and 12 nm (pore tip diameter). (d) Calculated $I-V$ curves at different $MgCl_2$ concentrations, $c_S = 0.1$ M KCl, and pH = 9. The current is scaled to a normalization current I_0 that depends on the nanopore and electrolyte solution characteristics.

gives $X_0 = 0.1$ M at the pore tip region, in agreement with our previous analysis for a similar nanopore.[14] Figure 5d shows the influence of the binding constant on the calculated $I-V$ curves for different $CaCl_2$ concentrations. This theoretical curve can be compared qualitatively with the experimental data of Figure 3b and suggests that the effective binding constant of calcium to the divalent phosphonic group should be on the order of 10^5 M^{-1}.

Figure 6 shows the calculated $I-V$ curves for the pore modified with APPA molecules in the absence and presence of calcium at different pH values. The currents have been scaled to a normalization current I_0 that depends on the pore geometry (the tip and base radii of the cone and its length), the maximum fixed charge concentration, and the electrolyte characteristics. It is clear that the theoretical curves are able to describe the observed experimental trends of Figure 2, which shows that continuum approaches can approximately describe the transport phenomena observed with these nanopores because the pore radii are much larger than the ionic size.[51]

While the model predicts qualitatively similar $I-V$ curves for different divalent ions, the decrease in the current with the ion concentration (Figure 3b) depends on the particular binding constant assumed (Figure 5d). Therefore, different divalent ions should show different blocking phenomena. Sensitivity to block by specific divalent ions is another characteristic of ion channels.[1] In particular, Mg^{2+} ion is also present in intracellular fluids and influences significantly the rectification phenomena in ion channels.[1]

Figure 7a shows the experimental $I-V$ curves of the APPA-modified pore obtained at fixed $MgCl_2$ concentration at different pH conditions. The results are qualitatively similar to those obtained in Figure 2b for $CaCl_2$. Figure 7b corresponds to the same pore in the absence and presence (concentration 10 mM) of divalent Mg^{2+} and Ca^{2+} ions at pH = 5. The results are similar for the two divalent ions (absence of current decrease at pH = 5). Finally, Figure 7c considers the case of different $MgCl_2$ concentrations at pH = 9, and Figure 7d shows the theoretically calculated $I-V$ curves. If we compare Figure 3b with Figure 7c, it becomes clear that the binding of Ca^{2+} to the pore fixed charges is stronger than the binding of Mg^{2+} (note also the different binding constants in Figures 5d and 7d). The different individual properties of divalent ions in solution determine also the degree of binding to specific sites observed in ion channels.[1] In particular, the dynamic nature of the effective hydration shells of Ca^{2+} and Mg^{2+} is significantly different,[53] and in the dissolved state, Mg^{2+}

binds hydration water tighter than that of Ca^{2+} ions. This fact could explain the relatively weak interaction of Mg^{2+} with the doubly charged phosphonate group.

CONCLUSIONS

We have presented a qualitative phenomenological description of the calcium binding to fixed charge groups confined over nanoscale regions and its influence on the ionic currents through a pore. The dissociation equilibrium and ionic transport in a single conical nanopore functionalized with pH-responsive carboxylic acid and phosphonic polyacid chains have been analyzed experimentally and theoretically. Different equilibrium and transport phenomena relevant to the ion channels of cell membranes and artificial nanopores are simultaneously present in this basic problem of physical and biophysical chemistry: (i) the charge state of the groups fixed to the pore and the influence of the pH and calcium on the reversible dissociation equilibrium of these groups; (ii) the asymmetry in the fixed charge density; and (iii) the effects of the applied potential difference and calcium concentration on the observed ionic currents. The physical models are based on simple but plausible assumptions and make use of well-established concepts of the statistical thermodynamics and transport phenomena of electrolyte solutions. The results should be of interest for the basic understanding of divalent ion binding and transport in biological ion channels and synthetic membranes.

MATERIALS AND METHODS

Polyethyleneterephthalate (PET) membranes (Hostaphan RN 12, Hoechst) with a thickness of 12 μm are irradiated at the Helmholtz Centre for Heavy Ion Research (GSI, Darmstadt) by single swift heavy Au ions of energy 11 MeV/u. The ion tracked PET membrane is then irradiated with UV light (50 W/m^2) for 15 min from each side to sensitize the latent tracks for the subsequent etching process. *N*-(3-Dimethylaminopropyl)-*N*′-ethylcarbodiimide hydrochloride (EDC, 98%, Fluka), pentafluorophenol (PFP, 99+%, Aldrich), and 3-aminopropylphosphonic acid (APPA; 99%, Aldrich) are then used in order to achieve the appropriate chemical modifications.

Fabrication of Single Conical Nanopores. The asymmetric track-etching technique by Apel *et al.* is employed to obtain the single conical nanopores in the PET membranes.[29] A single-shot PET membrane located between the two halves of the conductivity cell serves as a dividing wall between the left compartment filled with an etching solution (9 M NaOH) and right compartment with a stopping solution (1 M HCOOH + 1 M KCl). During the etching process occurring at room temperature, a potential difference of −1 V across the membrane gives a zero current, provided that the channel is not etched through. When the pore breakthrough occurs, a sudden increase in current to typically ~100 pA, together with significant current fluctuations, is observed. The stopping solution on the other side of the membrane then neutralizes the etchant coming from the left compartment of the cell. The etching process is terminated when the current is approximately stable and reaches a value of ~150−300 pA after a certain fixed interval of time. The etched pore is washed with a stopping solution to quench the etchant inside the nascent pore as well as with deionized water. Finally, the resulting membrane is immersed in deionized water overnight to remove all residual salts.

Immobilization of Polyprotic Acid Chains. Due to the ion irradiation and subsequent chemical etching process, carboxyl (COOH) groups are generated on the surface and inside walls of the pore. These COOH moieties constitute the sites that permit further pore functionalization by appropriate surface chemistry. To this end, the COOH groups of the pore surface are activated by carbodiimide coupling chemistry. In the activation process, ethanolic solutions of EDC (200 mM) and PFP (400 mM) are prepared separately and mixed together, achieving the final concentrations of 100 mM EDC and 200 mM PFP. Subsequently, the single-pore membrane is immersed for 60 min in the activation solution at room temperature. The surface COOH groups are then converted into amine-reactive pentafluorophenyl esters in this activation process. After washing with ethanol several times, the single-pore membrane is dipped in an aqueous ethanolic solution of 3-aminopropylphosphonic acid (20 mM) overnight, and reactive PFP esters are covalently coupled with the primary amine group of APPA in this process. Finally, the resulting membrane is washed with ethanol and deionized water.

Current−Voltage Measurements. The APPA-modified membrane is fixed between the two halves, forming the conductivity cell. The *I*−*V* curves are measured using a 100 mM KCl electrolyte solution at different pH values (adjusted by dilute HCl or NaOH solutions) in the two cell halves. Different concentrations of $CaCl_2$ and $MgCl_2$ can also be used in the electrolyte solutions. The Ag/AgCl electrodes are located in the respective half-cell solutions, and a picoammeter/voltage source is employed to apply the potential difference. The resulting ionic currents through the single pore are measured with a scanning triangle voltage (from −2 to +2 V) applied on the tip pore side, while the base side is connected to the ground electrode.

Conflict of Interest: The authors declare no competing financial interest.

Acknowledgment. P.R., J.C., and S.M. acknowledge the financial support from the Generalitat Valenciana (project PROMETEO/GV/0069), Ministry of Science and Innovation of Spain, Materials Program (project nos. MAT2009-07747 and MAT2012-32084), and FEDER. M.A., S.N., and W.E. gratefully acknowledge financial support by the Beilstein-Institut, Frankfurt/Main, Germany, within the research collaboration NanoBiC, and Prof. C. Trautmann (GSI, Department of Materials Research) for support with irradiation experiments.

REFERENCES AND NOTES

1. Hille, B. *Ionic Channels of Excitable Membranes*, 2nd ed.; Sinauer Associates Inc.: Sunderland, MA, 1991; Chapters 4−6, pp 83−169, and Chapter 18, pp 472−503.
2. Matulef, K.; Zagotta, W. N. Cyclic Nucleotide-Gated Ion Channels. *Annu. Rev. Cell Dev. Biol.* **2003**, *19*, 23–44.
3. Hackos, D. H.; Korenbrot, J. I. Divalent Cation Selectivity is a Function of Gating in Native and Recombinant Cyclic Nucleotide-Gated Ion Channels from Retinal Photoreceptors. *J. Gen. Physiol.* **1999**, *113*, 799–817.
4. Picones, A.; Korenbrot, J. I. Permeability and Interaction of Ca^{2+} with cGMP-Gated Ion Channels Differ in Retinal Rod and Cone Photoreceptors. *Biophys. J.* **1995**, *69*, 120–127.
5. Colamartino, G.; Menini, A.; Torre, V. Blockage and Permeation of Divalent Cations through the Cyclic GMP-Activated Channel from Tiger Salamander Retinal Rods. *J. Physiol.* **1991**, *440*, 189–206.
6. Eismann, E.; Muller, F.; Heinemann, S. H.; Kaupp, U. B. A Single Negative Charge Within the Pore Region of a cGMP-Gated Channel Controls Rectification, Ca^{2+} Blockage, and Ionic Selectivity. *Proc. Natl. Acad. Sci. U. S. A.* **1994**, *91*, 1109–1113.

7. Yau, K. W.; Baylor, D. A. Cyclic GMP-Activated Conductance of Retinal Photoreceptor Cells. *Annu. Rev. Neurosci.* **1989**, *12*, 289–327.
8. Methfessel, C.; Boheim, G. The Gating of Single Calcium-Dependent Potassium Channels Is Described by an Activation/Blockade Mechanism. *Biophys. Struct. Mech.* **1982**, *9*, 35–60.
9. Nonner, W.; Eisenberg, B. Ion Permeation and Glutamate Residues Linked by Poisson-Nernst-Planck Theory in L-Type Calcium Channels. *Biophys. J.* **1998**, *75*, 1287–1305.
10. Nonner, W.; Catacuzzeno, L.; Eisenberg, B. Binding and Selectivity in L-Type Calcium Channels: A Mean Spherical Approximation. *Biophys. J.* **2000**, *79*, 1976–1992.
11. Verdiá-Báguena, C.; Queralt-Martín, M.; Aguilella, V. M.; Alcaraz, A. Protein Ion Channels as Molecular Ratchets. Switchable Current Modulation in Outer Membrane Protein F Porin Induced by Millimolar La^{3+} Ions. *J. Phys. Chem. C* **2012**, *116*, 6537–6542.
12. Hou, X.; Zhang, H. C.; Jiang, L. Building Bio-Inspired Artificial Functional Nanochannels: From Symmetric to Asymmetric Modification. *Angew. Chem., Int. Ed.* **2012**, *51*, 5296–5307.
13. Garcia-Gimenez, E.; Alcaraz, A.; Aguilella, V. M.; Ramirez, P. Directional Ion Selectivity in a Biological Nanopore with Bipolar Structure. *J. Membr. Sci.* **2009**, *331*, 137–142.
14. Ali, M.; Mafe, S.; Ramirez, P.; Neumann, R.; Ensinger, W. Logic Gates Using Nanofluidic Diodes Based on Conical Nanopores Functionalized with Polyprotic Acid Chains. *Langmuir* **2009**, *25*, 11993–11997.
15. Ali, M.; Ramirez, P.; Mafe, S.; Neumann, R.; Ensinger, W. A pH-Tunable Nanofluidic Diode with a Broad Range of Rectifying Properties. *ACS Nano* **2009**, *3*, 603–608.
16. Ali, M.; Ramirez, P.; Tahir, M. N.; Mafe, S.; Siwy, Z.; Neumann, R.; Tremel, W.; Ensinger, W. Biomolecular Conjugation inside Synthetic Polymer Nanopores *via* Glycoprotein-Lectin Interactions. *Nanoscale* **2011**, *3*, 1894–1903.
17. Fan, R.; Karnik, R.; Yue, M.; Li, D. Y.; Majumdar, A.; Yang, P. D. DNA Translocation in Inorganic Nanotubes. *Nano Lett.* **2005**, *5*, 1633–1637.
18. He, Y.; Gillespie, D.; Boda, D.; Vlassiouk, I.; Eisenberg, R. S.; Siwy, Z. S. Tuning Transport Properties of Nanofluidic Devices with Local Charge Inversion. *J. Am. Chem. Soc.* **2009**, *131*, 5194–5202.
19. Healy, K.; Schiedt, B.; Morrison, A. P. Solid-State Nanopore Technologies for Nanopore-Based DNA Analysis. *Nanomedicine* **2007**, *2*, 875–897.
20. Kalman, E. B.; Vlassiouk, I.; Siwy, Z. S. Nanofluidic Bipolar Transistors. *Adv. Mater.* **2008**, *20*, 293–297.
21. Karnik, R.; Castelino, K.; Fan, R.; Yang, P.; Majumdar, A. Effects of Biological Reactions and Modifications on Conductance of Nanofluidic Channels. *Nano Lett.* **2005**, *5*, 1638–1642.
22. Ku, J. R.; Lai, S. M.; Ileri, N.; Ramirez, P.; Mafe, S.; Stroeve, P. pH and Ionic Strength Effects on Amino Acid Transport through Au-Nanotubule Membranes Charged with Self-Assembled Monolayers. *J. Phys. Chem. C* **2007**, *111*, 2965–2973.
23. Ramirez, P.; Apel, P. Y.; Cervera, J.; Mafe, S. Pore Structure and Function of Synthetic Nanopores with Fixed Charges: Tip Shape and Rectification Properties. *Nanotechnology* **2008**, *19*, 315707.
24. Ramirez, P.; Gomez, V.; Cervera, J.; Schiedt, B.; Mafe, S. Ion Transport and Selectivity in Nanopores with Spatially Inhomogeneous Fixed Charge Distributions. *J. Chem. Phys.* **2007**, *126*, 194703.
25. Siwy, Z. S.; Powell, M. R.; Kalman, E.; Astumian, R. D.; Eisenberg, R. S. Negative Incremental Resistance Induced by Calcium in Asymmetric Nanopores. *Nano Lett.* **2006**, *6*, 473–477.
26. Siwy, Z. S.; Powell, M. R.; Petrov, A.; Kalman, E.; Trautmann, C.; Eisenberg, R. S. Calcium-Induced Voltage Gating in Single Conical Nanopores. *Nano Lett.* **2006**, *6*, 1729–1734.
27. Queralt-Martin, M.; Garcia-Gimenez, E.; Mafe, S.; Alcaraz, A. Divalent Cations Reduce the pH Sensitivity of OmpF Channel Inducing the pK(a) Shift of Key Acidic Residues. *Phys. Chem. Chem. Phys.* **2011**, *13*, 563–569.
28. Innes, L.; Powell, M. R.; Vlassiouk, I.; Martens, C.; Siwy, Z. S. Precipitation-Induced Voltage-Dependent Ion Current Fluctuations in Conical Nanopores. *J. Phys. Chem. C* **2010**, *114*, 8126–8134.
29. Apel, P. Y.; Korchev, Y. E.; Siwy, Z.; Spohr, R.; Yoshida, M. Diode-Like Single-Ion Track Membrane Prepared by Electro-Stopping. *Nucl. Instrum. Methods Phys. Res., Sect. B* **2001**, *184*, 337–346.
30. Ali, M.; Nasir, S.; Nguyen, Q. H.; Sahoo, J. K.; Tahir, M. N.; Tremel, W.; Ensinger, W. Metal Ion Affinity-Based Biomolecular Recognition and Conjugation inside Synthetic Polymer Nanopores Modified with Iron-Terpyridine Complexes. *J. Am. Chem. Soc.* **2011**, *133*, 17307–17314.
31. Ali, M.; Nasir, S.; Ramirez, P.; Ahmed, I.; Nguyen, Q. H.; Fruk, L.; Mafe, S.; Ensinger, W. Optical Gating of Photosensitive Synthetic Ion Channels. *Adv. Funct. Mater.* **2012**, *22*, 390–396.
32. Ali, M.; Ramirez, P.; Nguyen, H. Q.; Nasir, S.; Cervera, J.; Mafe, S.; Ensinger, W. Single Cigar-Shaped Nanopores Functionalized with Amphoteric Amino Acid Chains: Experimental and Theoretical Characterization. *ACS Nano* **2012**, *6*, 3631–3640.
33. Hou, X.; Jiang, L. Learning from Nature: Building Bio-Inspired Smart Nanochannels. *ACS Nano* **2009**, *3*, 3339–3342.
34. Vlassiouk, I.; Siwy, Z. S. Nanofluidic Diode. *Nano Lett.* **2007**, *7*, 552–556.
35. Wanunu, M.; Meller, A. Chemically Modified Solid-State Nanopores. *Nano Lett.* **2007**, *7*, 1580–1585.
36. Powell, M. R.; Sullivan, M.; Vlassiouk, I.; Constantin, D.; Sudre, O.; Martens, C. C.; Eisenberg, R. S.; Siwy, Z. S. Nanoprecipitation-Assisted Ion Current Oscillations. *Nat. Nanotechnol.* **2008**, *3*, 51–57.
37. Zhang, J.; Kirkham, J.; Robinson, C.; Wallwork, M. L.; Smith, D. A.; Marsh, A.; Wong, M. Determination of the Ionization State of 11-Thioundecyl-1-Phosphonic Acid in Self-Assembled Monolayers by Chemical Force Microscopy. *Anal. Chem.* **2000**, *72*, 1973–1978.
38. Jaskari, T.; Vuorio, M.; Kontturi, K.; Manzanares, J. A.; Hirvonen, J. Ion-Exchange Fibers and Drugs: An Equilibrium Study. *J. Controlled Release* **2001**, *70*, 219–229.
39. Ramirez, P.; Alcaraz, A.; Mafe, S.; Pellicer, J. Donnan Equilibrium of Ionic Drugs in pH-Dependent Fixed Charge Membranes: Theoretical Modeling. *J. Colloid Interface Sci.* **2002**, *253*, 171–179.
40. Minagawa, M.; Tanioka, A.; Ramirez, P.; Mafe, S. Amino Acid Transport Through Cation Exchange Membranes: Effects of pH on Interfacial Transport. *J. Colloid Interface Sci.* **1997**, *188*, 176–182.
41. Dydek, E. V.; Zaltzman, B.; Rubinstein, I.; Deng, D. S.; Mani, A.; Bazant, M. Z. Overlimiting Current in a Microchannel. *Phys. Rev. Lett.* **2011**, *107*, 118301.
42. Kontturi, K.; Murtomäki, L.; Manzanares, J. A., *Ionic Transport Processes*; Oxford University: Oxford, 2008; Chapter 2, pp 38−76.
43. Charman, W. N.; Christy, D. P.; Geunin, E. P.; Monkhouse, D. C. Interaction Between Calcium, a Model Divalent Cation, and a Range of Poly (Acrylic Acid) Resins as a Function of Solution pH. *Drug Dev. Ind. Pharm.* **1991**, *17*, 271–280.
44. Ramirez, P.; Mafe, S.; Aguilella, V. M.; Alcaraz, A. Synthetic Nanopores with Fixed Charges: An Electrodiffusion Model for Ionic Transport. *Phys. Rev. E* **2003**, *68*, 011910.
45. Mafe, S.; Garcia-Morales, V.; Ramirez, P. Estimation of pK(a) Shifts in Weak Polyacids Using a Simple Molecular Model: Effects of Strong Polybases, Hydrogen Bonding and Divalent Counterion Binding. *Chem. Phys.* **2004**, *296*, 29–35.
46. Cervera, J.; Alcaraz, A.; Schiedt, B.; Neumann, R.; Ramirez, P. Asymmetric Selectivity of Synthetic Conical Nanopores Probed by Reversal Potential Measurements. *J. Phys. Chem. C* **2007**, *111*, 12265–12273.

47. Cervera, J.; Ramirez, P.; Mafe, S.; Stroeve, P. Asymmetric Nanopore Rectification for Ion Pumping, Electrical Power Generation, and Information Processing Applications. *Electrochim. Acta* **2011**, *56*, 4504–4511.
48. English, A. E.; Mafe, S.; Manzanares, J. A.; Yu, X. H.; Grosberg, A. Y.; Tanaka, T. Equilibrium Swelling Properties of Polyampholytic Hydrogels. *J. Chem. Phys.* **1996**, *104*, 8713–8720.
49. Hill, T. L. *Cooperative Theory in Biochemistry*; Springer: New York, 1985; Chapters 1 and 2.
50. Ben-Naim, A. *Cooperativity and Regulation in Biochemical Processes*; Kluwer Academic/Plenum: New York, 2001; Chapter 1, pp 1−20.
51. Cervera, J.; Ramirez, P.; Manzanares, J. A.; Mafe, S. Incorporating Ionic Size In the Transport Equations for Charged Nanopores. *Microfluid. Nanofluid.* **2010**, *9*, 41–53.
52. Cervera, J.; Schiedt, B.; Neumann, R.; Mafe, S.; Ramirez, P. Ionic Conduction, Rectification, and Selectivity in Single Conical Nanopores. *J. Chem. Phys.* **2006**, *124*, 104706.
53. Hille, B. *Ionic Channels of Excitable Membranes*, 2nd ed.; Sinauer Associates Inc.: Sunderland, MA, 1991; Chapter 10, pp 261−290.